scientific reports

Check for updates

OPEN

Rapid retinoic acid-induced trophoblast cell model from human induced pluripotent stem cells

Kristen A. Lemke[1], Casim A. Sarkar[2] & Samira M. Azarin[1]✉

A limited number of accessible and representative models of human trophoblast cells currently exist for the study of placentation. Current stem cell models involve either a transition through a naïve stem cell state or precise dynamic control of multiple growth factors and small-molecule cues. Here, we demonstrated that a simple five-day treatment of human induced pluripotent stem cells with two small molecules, retinoic acid (RA) and Wnt agonist CHIR 99021 (CHIR), resulted in rapid, synergistic upregulation of CDX2. Transcriptomic analysis of RA + CHIR-treated cells showed high similarity to primary trophectoderm cells. Multipotency was verified via further differentiation towards cells with syncytiotrophoblast or extravillous trophoblast features. RA + CHIR-treated cells were also assessed for the established criteria defining a trophoblast cell model, and they possess all the features necessary to be considered valid. Collectively, our data demonstrate a facile, scalable method for generating functional trophoblast-like cells in vitro to better understand the placenta.

The human placenta is a vital, transient organ responsible for mechanical attachment and nutrient exchange between the mother and the developing fetus. Following embryo implantation, trophectoderm cells segregate from inner cell mass (ICM) cells, giving rise to mononuclear cytotrophoblast (CTB) cells, which are considered trophoblast stem cells (TSCs). The CTB cells give rise to two types of specialized placental cells: hormone-secreting multinucleated syncytiotrophoblast (STB) cells and the invasive extravillous trophoblast (EVT) cells[1]. Though little is known about how this cascade of events unfolds in early human embryos, complications with placentation are thought to underpin the mechanisms involved in preeclampsia, intrauterine growth restriction, and miscarriages[2]. Therefore, it has been of significant interest to better understand how the human placenta is initially formed.

Current models of the early human placenta include primary cells, murine trophoblast cells, and stem cell-derived trophoblast cells. Primary human trophoblast stem cells (hTSCs) have been isolated and characterized from both blastocysts and first trimester placentas[3], but important ethical and regulatory barriers protecting early gestation limit the ability to establish new hTSC lines for patient-specific or genetic disease modeling. Choriocarcinoma cell lines (e.g., BeWo and JEG-3) are also used to model the placenta, but these cells do not represent healthy placental tissue[4]. Recently, methods to transition directly from primary human fibroblasts to hTSCs have been reported, allowing for genetically diverse, patient-specific placental models[5,6]. However, the sophisticated viral reprogramming techniques involved in these methods exceed the capabilities of many research groups, and heterogeneous populations following transduction can necessitate manual selection steps. Murine trophoblast cells have also been used to model the human placenta but contain additional subtype populations when compared to human populations. Additionally, mouse trophoblast cell development deviates from the human counterpart in numerous ways, one of which being the importance of Oct-4 in inducing CDX2 expression in human systems, rendering murine models inadequate for understanding early cell-fate decisions in human cells[1,2,7–9]. Collectively, these shortcomings have led to exploration of alternative approaches, including models generated from human pluripotent stem cells (hPSCs).

Initially, induced expression of key trophoblast cell transcription factors or treatment with key signaling molecules was shown to initiate a trophoblast cell fate[10–12]. Most commonly, hPSCs treated with bone morphogenetic protein 4 (BMP-4) have been used as a model of trophoblast cells as these cells acquire many trophoblast cell features, including expression of keratin 7 (*KRT7*) and secretion of human chorionic gonadotropin (hCG)[12,13]. However, subsequent studies using mouse cells concluded that in vitro differentiation of trophoblast cells from embryonic stem cells was incomplete, inferring that trophoblast cells and embryonic

[1]Department of Chemical Engineering and Materials Science, University of Minnesota, Minneapolis, MN 55455, USA. [2]Department of Biomedical Engineering, University of Minnesota, Minneapolis, MN 55455, USA. ✉email: azarin@umn.edu

stem cells represent two distinct lineages both arising from the blastocyst[14]. For this reason, the validity of stem cell-derived models in recapitulating human trophoblast cells has been controversial[15], prompting experts to define a set of criteria—expression of *ELF5*; chromosome-19 microRNA cluster (C19MC) miRNA expression; *KRT7*, *TFAP2C*, and *GATA3* expression; and *HLA-G* expression—for a high-fidelity trophoblast cell model[16]. Recent improvements in methods of BMP-4-induced hPSC differentiation towards trophoblast cells have led to generation of a population termed human trophectoderm stem cells (hTESCs) under chemically defined conditions, with multiple interacting protein and small-molecule cues required[17]. It has also been hypothesized that utilizing a naïve hPSC population may improve differentiation to trophoblast cells, since naïve stem cells may possess a greater potential for trophoblast cell differentiation when compared to primed stem cells, including traditional stem cell lines[18,19]. Transitioning primed stem cells to a naïve state prior to subsequent differentiation has been shown to improve expression of trophoblast cell markers, but this additional transition step takes weeks[18].

Here we present a rapid, simple platform for the generation of human trophoblast cells from human induced pluripotent stem cells (hiPSCs) by administration of retinoic acid (RA) and the canonical Wnt signaling agonist CHIR 99021 (CHIR). Both the RA and Wnt signaling pathways have previously been implicated in the development of extra-embryonic tissue, but RA and Wnt agonists have not been used in combination nor has their use on stem cells been compared to current BMP-4-induced model trophoblast cells[20,21]. We demonstrate that hiPSCs treated with RA and CHIR quickly adopt features similar to primary trophectoderm cells, are comparable to hPSC-derived trophoblast cell models, and meet the established criteria for trophoblast cell models.

Results

hiPSC treatment with small molecules RA and CHIR leads to trophoblast cell differentiation

First, we treated IMR90-4 hiPSCs with 1 μM retinoic acid (RA) in unconditioned medium (UM) (Fig. 1a). After 5 days of RA treatment, the cells lost expression of the pluripotency marker Oct-4 and gained expression of both keratin 18, an epithelial marker, and CDX2, an early marker of the human placenta (Figs. 1b,c, S1)[22]. Though CDX2 expression in human trophectoderm (TE) has been reported to be variable and low, its expression distinguishes the cells of the TE from those of the ICM and primitive endoderm (PE) as early as

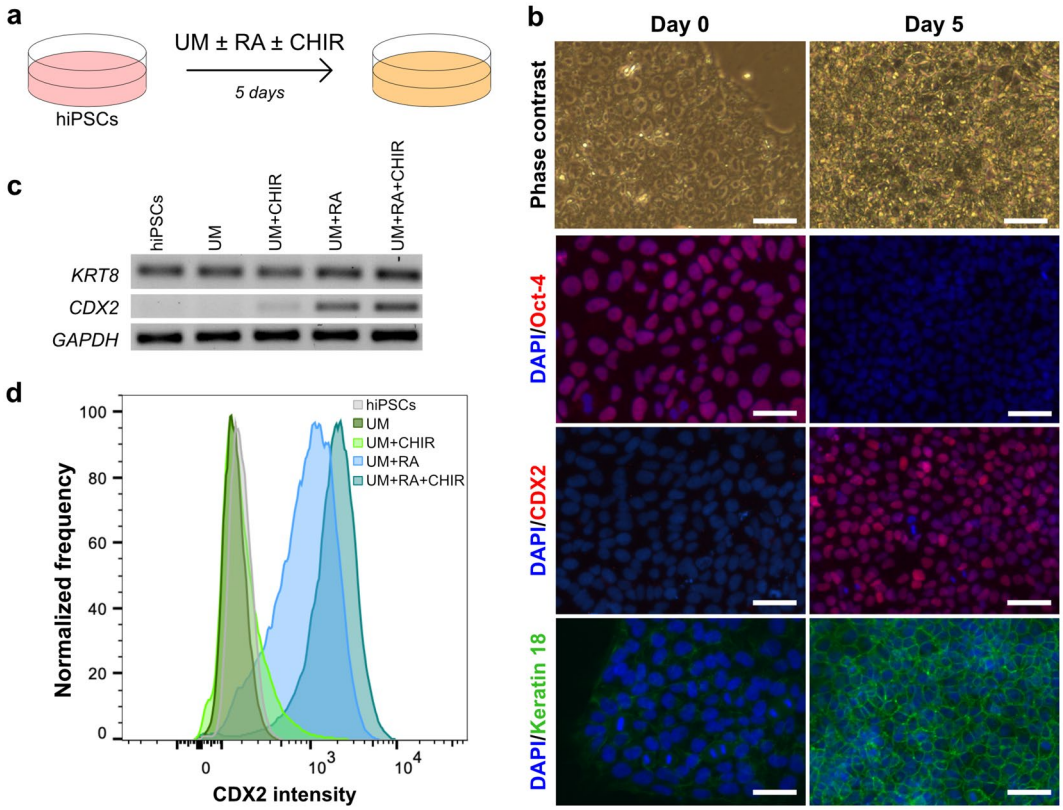

Figure 1. Treatment with both RA and CHIR results in consistent upregulation of CDX2. (**a**) Schematic diagram of differentiation. (**b**) Phase contrast and immunostaining images of cells before (Day 0) and following (Day 5) RA treatment. (**c**) RT-PCR of cells before treatment (hiPSCs) and cells treated for 5 days with conditions denoted above gel. *GAPDH* was used as a control. Original gel is presented in Fig. S4. (**d**) Representative flow cytometric histograms of CDX2 expression in cells before treatment (hiPSCs) or cells treated for 5 days with conditions denoted in legend. Scale bars are 50 μm.

5 days post-fertilization[23]. We also confirmed morphological characteristics of epithelial cells including merging colonies, confluent monolayers with polygonal morphology, and tight cell-to-cell interactions (Fig. 1b, S2)[24]. The addition of 8 μM CHIR to the RA-containing medium increased CDX2 expression compared to RA-only conditions (Figs. 1d, S3). As expected, the addition of CHIR, which acts as a canonical Wnt agonist by stabilizing beta-catenin, increased active beta-catenin within the cells (Fig. S3), but CHIR alone was insufficient to promote expression of CDX2 in the absence of RA (Fig. 1c, S3). When 5 μM IWP2, a canonical Wnt antagonist, was added to the culture in the presence of RA, the total amount of active beta-catenin was reduced when compared to RA alone (Fig. S3). The addition of IWP2 also caused a reduction in the expression of CDX2 when compared to RA alone, but did not completely abrogate its expression, which indicated a role of active beta-catenin in maintaining expression of CDX2 (Fig. S3).

We also quantitatively confirmed higher CDX2 expression in RA + CHIR-treated cells than in RA-treated cells (median expression intensities of 1988 ± 68 vs. 1348 ± 42, respectively, $p < 0.001$, Fig. 1d). The addition of CHIR also decreased the variability of CDX2 expression compared to RA alone, as visually evident from the overall CDX2 expression distributions (Fig. 1d) and as measured by the interquartile range (IQR) of CDX2 fluorescence intensity (IQR of 119 for RA alone vs. 81 for RA + CHIR).

Temporal analysis reveals emergence of trophoblast cell-specific markers

Along with increased expression of *CDX2*, we observed significant upregulation of transcription factors *GATA3* and *KLF4* and the trophoblast cell-specific keratin 7 (*KRT7*)[16,25] by days 4 and 5 of differentiation (Fig. 2a,b). GATA-binding factor 3 (GATA3) has been well established as a TE transcription factor and was previously shown to promote expression of placental genes and downregulate the pluripotency program in human cells[26]. Krüppel-like factor 4 (KLF4) has been shown to regulate expression of pregnancy-specific glycoproteins (PSGs), specifically PSG-5[27]. We also confirmed expression of E-cadherin, GATA3, and keratin 7 via immunocytochemistry in cells treated with RA + CHIR for five days, indicating an epithelial trophoblast cell type (Fig. 2c). Expression of E-cadherin, GATA3, and keratin 7 was also observed in two additional hiPSC lines (ACS-1024 hiPSCs and UMN PCBC16iPS) treated with RA + CHIR for five days, demonstrating robustness of the protocol (Fig. S5). Furthermore, primary human trophoblast cells are known to transiently co-express lineage-specific transcription factors Oct-4 and CDX2[22]. Using flow cytometry, we saw emergence of a $CDX2^+/Oct\text{-}4^+$ population after 3 days of incubation in RA + CHIR, which transitioned to $CDX2^+/Oct\text{-}4^-$ by day 5 (Fig. 2d).

To further characterize the trophoblast-like cells, we quantified the expression of microRNAs (miRNAs) from the chromosome-19 miRNA cluster (C19MC), expression of which has previously been shown to be restricted only to placental cells in adult tissues[28]. Previous BMP-4-derived trophoblast cell models had significantly lower expression (up to 4,000-fold lower) of C19MC miRNAs when compared to choriocarcinoma cells[16,29]. In day 5 RA + CHIR-treated cells, qRT-PCR analysis revealed that expression of C19MC miRNAs *517a* and *517b* was greatly improved relative to BMP-4 models to levels within an order of magnitude (~ tenfold) of those of BeWo choriocarcinoma cells, and expression of miRNAs *525-3p* and *526b-3p* remained high in day 5 RA + CHIR-treatment at levels consistent with BeWo cells (Fig. 2e). These results indicate the RA + CHIR-treated cells demonstrate improved agreement with the established criteria of a trophoblast cell model.

RNA sequencing shows RA + CHIR-treated cells have high transcriptional correlation with early primary trophectoderm cells

To broadly characterize the identity of the cells generated from RA and CHIR treatment, we performed bulk RNA sequencing. Differential gene expression analysis between hiPSCs (day 0) and day 5 RA + CHIR-treated cells revealed that several key pathways were upregulated including Wnt signaling, sphingosine-1-phosphate (S1P) signaling, and vitamin D3 receptor/retinoid X receptor (VDR/RXR) signaling (Table S1). Furthermore, we observed cholesterol biosynthesis pathways were downregulated, along with the epithelial mesenchymal transition (EMT) pathway and signal transducer and activator of transcription 3 (STAT3) signaling (Table S2). Upstream regulator analysis revealed that BMP-4 activates several of the key species observed to be differentially expressed between day 0 and day 5, indicating a potential similarity in the mechanisms of BMP-4-derived trophoblast cell models and RA + CHIR-treated cells (Table S3).

We compared RA + CHIR-treated cell RNA-sequencing data with averaged single-cell RNA-sequencing data obtained from human embryo-derived epiblast (EPI), primitive endoderm (PE), and trophectoderm (TE) on days 6 through 14 (D6-D14) post-implantation (GSE109555)[30] and two alternative hPSC differentiation methods to generate trophoblast cell models (GSE138762 and GSE137295)[17,18]. The GSE138762 dataset included both naïve and primed trophoblast stem cells (TSCs) that were generated from differentiation of a naïve or primed population of stem cells, respectively. The GSE137295 dataset included human trophoblast stem cells (hTSCs), similar to BMP-4-induced naïve TSCs, hTESCs, and human trophoblast stem cell lines CT29 and CT30 (Fig. 3).

Principal component analysis revealed RA + CHIR-treated cells clustered close to epiblast cells of the inner cell mass at early time points (day 0 and day 1), but by day 5, the RA + CHIR cells developed a positive PC2 signature, akin to the primary TE samples (Fig. 4a). Spearman correlation analysis also demonstrated that the day 5 RA + CHIR-treated cells are most like TE when compared to other early embryonic structures like epiblast and primitive endoderm (Fig. S6). Next, we compared the RA + CHIR method to two other differentiation protocols to determine how close the various differentiated cell populations clustered to primary TE cells. Day 5 RA + CHIR cells cluster with all the primary TE samples when analyzed using k-means clustering, unlike the majority of samples from alternative differentiation approaches (Fig. 4b). Spearman correlation analysis of the analyzed stem cell models along with the primary TE data revealed day 5 RA + CHIR cells clustered closest to day 6 and day 8 primary TE and distinctly from primed TSCs and other stem cell-derived models (Fig. S7).

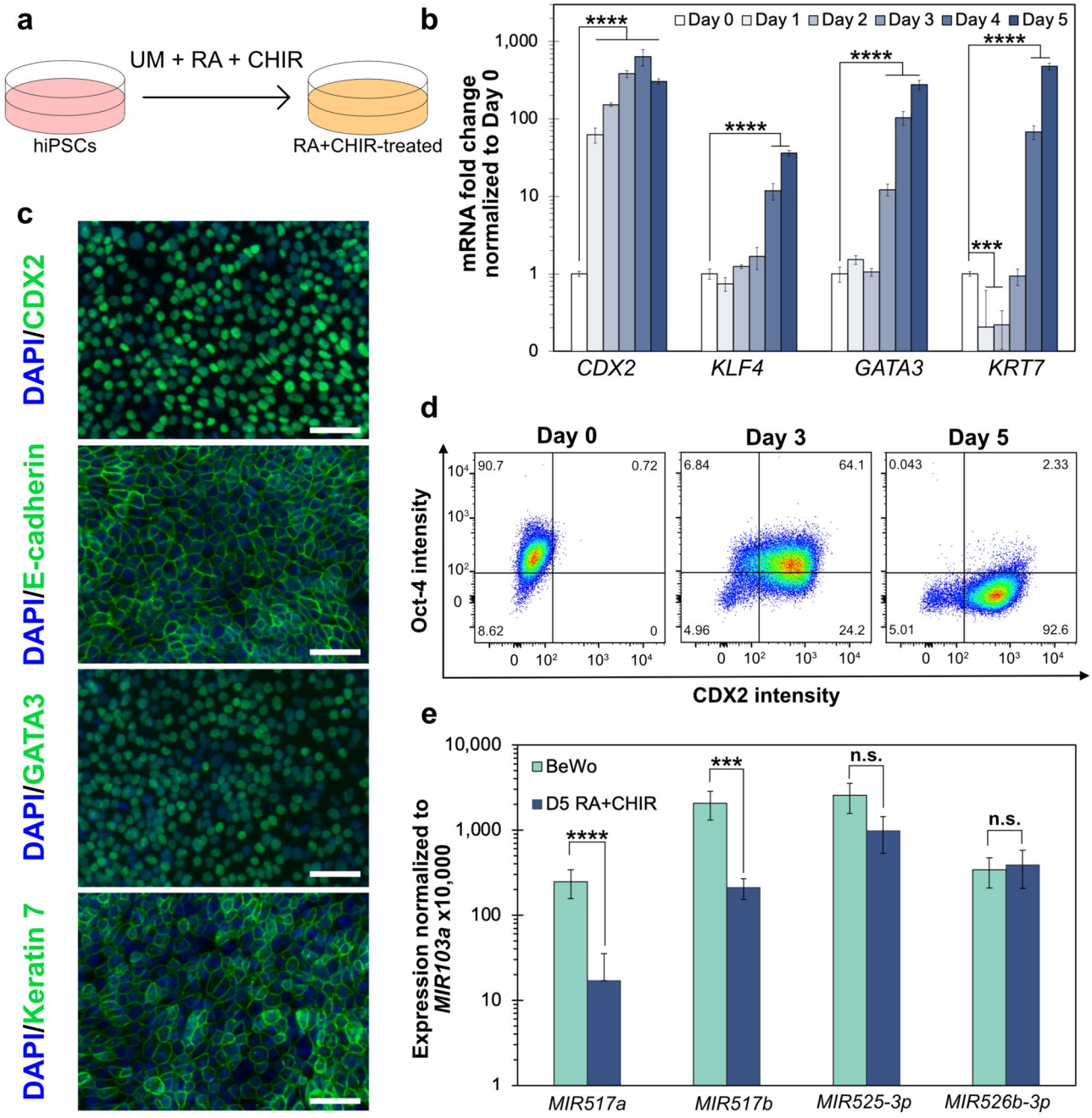

Figure 2. RA and CHIR treatment induces expression of markers associated with trophoblast cell differentiation. (**a**) Schematic diagram of the differentiation. (**b**) qRT-PCR analysis during the differentiation in UM containing RA + CHIR. (**c**) Immunocytochemistry of cells treated for 5 days with UM containing RA + CHIR. (**d**) CDX2 and Oct-4 expression as determined by flow cytometry at the indicated timepoints during differentiation. Numeric values in each corner represent the percent of cells within each quadrant. (**e**) qRT-PCR analysis of C19 microRNAs during differentiation. Data are presented as mean ± SD of three independent replicates. Scale bars in images are 50 µm. n.s. = not significant, *p ≤ 0.05, **p ≤ 0.01, ***p ≤ 0.001, ****p ≤ 0.0001 based on ANOVA of three independent experimental replicates.

When we looked specifically at genes associated with TE cell development[30–33], we saw that within 5 days, RA + CHIR-treated cells express many genes associated with early TE, but do not express some genes associated with mature trophoblast cells (e.g., *PSG* family, Fig. 4c). Differential gene expression analysis demonstrated that day 5 RA + CHIR-treated cells expressed lower levels of beta subunit chorionic gonadotropins (CGBs) than hTESCs, hTSCs, and the trophoblast stem cell line CT29 (Fig. S8). Compared to hTESCs, RA + CHIR-treated cells expressed significantly higher levels of *HLA-G* and *VGLL1* (Fig. S8). We also assessed the RA + CHIR-treated cells for genes associated with primitive endoderm, pluripotency maintenance, primordial germ cells (PGCs), and the three germ layers (endoderm, mesoderm, and ectoderm), and observed expression patterns consistent with genes expressed in primary TE or alternate hPSC-derived approaches (Figs. S9-S11). Furthermore, we compared

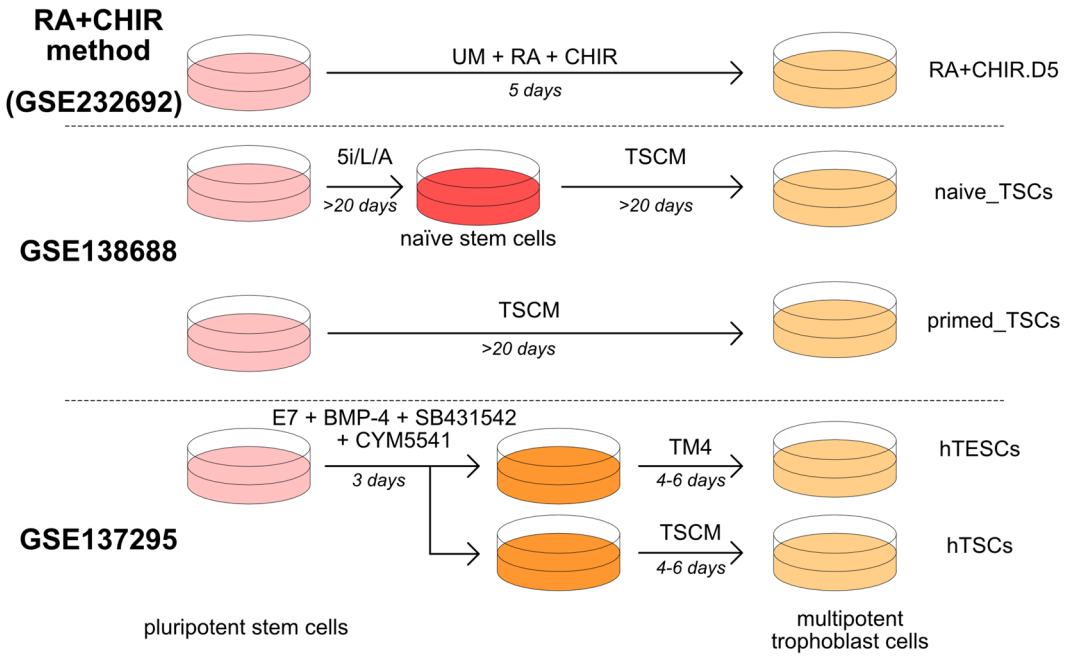

Figure 3. Methods, reagents, and nomenclature for alternative pluripotent stem cell differentiations to trophoblast cells. Schematic diagrams of differentiation methods and corresponding labels and GEO reference codes used for comparison in RNA-sequencing analysis. See Table S4 for media compositions.

the expression of a subset of amnion-associated genes in RA + CHIR-treated cells, primary TE, trophoblast stem cell lines (CT29 and CT30), and other stem cell-derived trophoblast cell models (Fig. S12). Expression of *VIM* and *CDH10* was low in RA + CHIR-treated cells, consistent with primary TE, but expression of *ISL1* was elevated when compared to primary TE, consistent with expression in hTESCs (Fig. S12).

Finally, we looked at the expression levels of two genes strongly implicated in human trophoblast cell development: *TFAP2C* and *ELF5*[16]. Day 5 RA + CHIR-treated cells had high expression of *TFAP2C*, consistent with both naïve TSC and hTSC populations, but had significantly higher expression than primed TSCs and hTESCs (Fig. 4d). Similarly, day 5 RA + CHIR-treated cells had high *ELF5* expression, consistent with the naïve TSCs, but significantly higher expression than primed TSCs, hTSCs, and hTESCs (Fig. 4e). Taken together, these data demonstrate that cells generated from treatment with RA + CHIR follow a similar temporal transcriptional profile as days 6–8 primary TE cells and express *ELF5* and *TFAP2C* at transcript levels similar to, if not higher than, alternative stem cell-derived models of the placenta.

RA + CHIR-treated cells demonstrate the capacity for further differentiation toward functional subtypes

To determine if the RA + CHIR-treated cells had potential for further differentiation to functional trophoblast cell subtypes, we subcultured the day 5 RA + CHIR cells and maintained them in either normoxia (20% O_2) or hypoxia (2% O_2) for 5 days (Fig. 5a). Cells in normoxia were expected to acquire STB-like features such as hCG expression and multinucleation, whereas cells in hypoxia were expected to acquire EVT-like features including proliferation, mesenchymal gene expression, and HLA-G1 expression[22]. We saw no expression of CDX2 in either STB-like or EVT-like cells, which is consistent with reports that CDX2 expression is lost as trophoblast cells differentiate (Fig. 5b)[22,34]. As expected, cells cultured in hypoxia had an increased number of Ki-67$^+$ cells, an indication the EVT-like cells were more proliferative than the STB-like cells cultured in normoxia (Fig. 5b). We also observed multinucleation in STB-like cells cultured under normoxic conditions, evident by multiple nuclei present inside cells labelled with membrane-localized E-cadherin (e.g., Fig. 5b, white arrows). The fusion index was significantly higher in the STB-like cells than the EVT-like cells (34 ± 4% and 14 ± 4%, respectively, Fig. 5c). We also observed expression of keratin 7 in both the EVT-like and STB-like cells (Fig. 5b). Furthermore, EVT-like cells demonstrated evidence of enhanced migration when compared to STB-like cells as assessed by a wound healing assay (53 ± 15% and 26 ± 6% wound closure, respectively, Fig. 5d,e).

We next looked at expression of HLA-G in the EVT-like cells. EVT cells are known to express the membrane-bound isoform of HLA-G, HLA-G1/5[16,35]. We saw an increase in transcript level expression of *HLA-G1/5* in EVT-like cells differentiated in hypoxia (Fig. 6a). Expression of *HLA-G* was also confirmed in two additional hiPSC lines that underwent differentiation with RA and CHIR, again an indication that this protocol is robust and reproducible across multiple hiPSC lines (Fig. S13). We further evaluated expression of epithelial and mesenchymal associated genes, as the transition from an epithelial to a mesenchymal phenotype (EMT) is a feature of EVT cells[33,36]. Expression of epithelial associated genes *TJP1* and *OCLN* showed significant downregulation when compared to day 5 RA + CHIR-treated cells (Fig. 6b). Conversely, mesenchymal associated

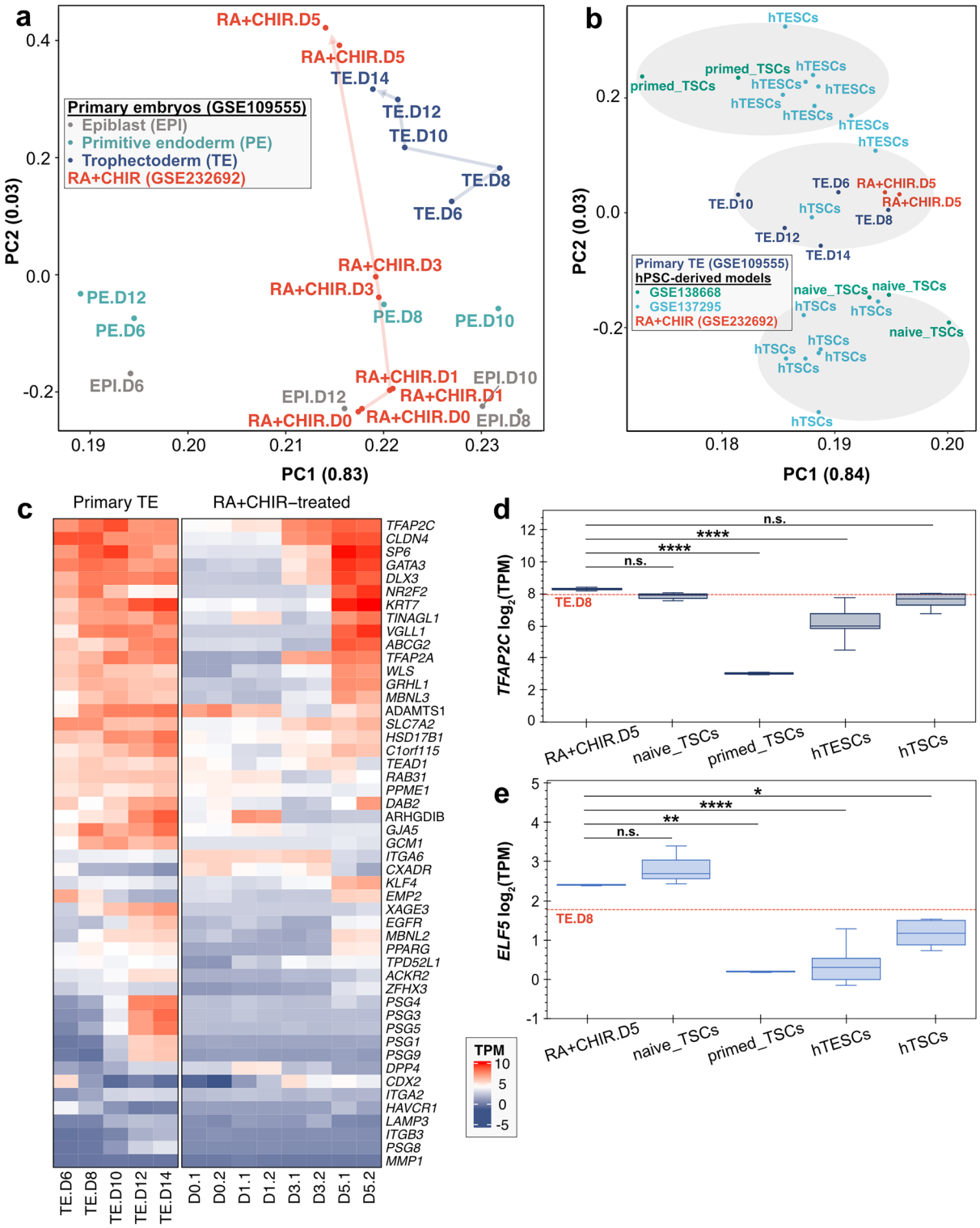

Figure 4. Transcriptional analysis of RA + CHIR treated cells reveals similarity to primary trophectoderm cells and previously established trophoblast cell models. (**a**) PCA of transcript level data from primary human embryo cells (epiblast: EPI.D6-D12, primitive endoderm: PE.D6-D12, trophectoderm: TE.D6-D14) and cells treated with RA + CHIR (RA + CHIR.D0-D5). Arrows were added for clarity and do not indicate known trajectory. Fraction of variance captured by each PC is included in parentheses. (**b**) PCA of transcript level data from primary human trophectoderm cells (TE.D6-D14), RA + CHIR treated cells (RA + CHIR.D5), and two alternative hPSC-derived differentiations (hTSCs, hTESCs, naïve_TSCs, primed_TSCs). Shaded regions indicate distinct k-means clusters. (**c**) Heatmap of $\log_2$(TPM) expression of genes associated with trophectoderm development in primary trophectoderm (TE.D6-D14) and in cells treated with RA + CHIR (D0.1 and D0.2 represent day 0 replicates 1 and 2, respectively). Heatmap was generated using the ComplexHeatmap package (2.20.0, https://github.com/jokergoo/ComplexHeatmap/) available from Bioconductor. (**d**,**e**) Log_2(TPM) expression of *TFAP2C* (**d**) and *ELF5* (**e**) in RNA-sequencing samples. Red dashed lines indicate expression level in day 8 primary trophectoderm (TE.D8). Data are presented as boxplots of independent replicates shown where applicable. Significance is determined based on comparison to RA + CHIR.D5. n.s. = not significant, * $p \le 0.05$, ** $p \le 0.01$, *** $p \le 0.001$, **** $p \le 0.0001$ based on ANOVA of independent experimental replicates.

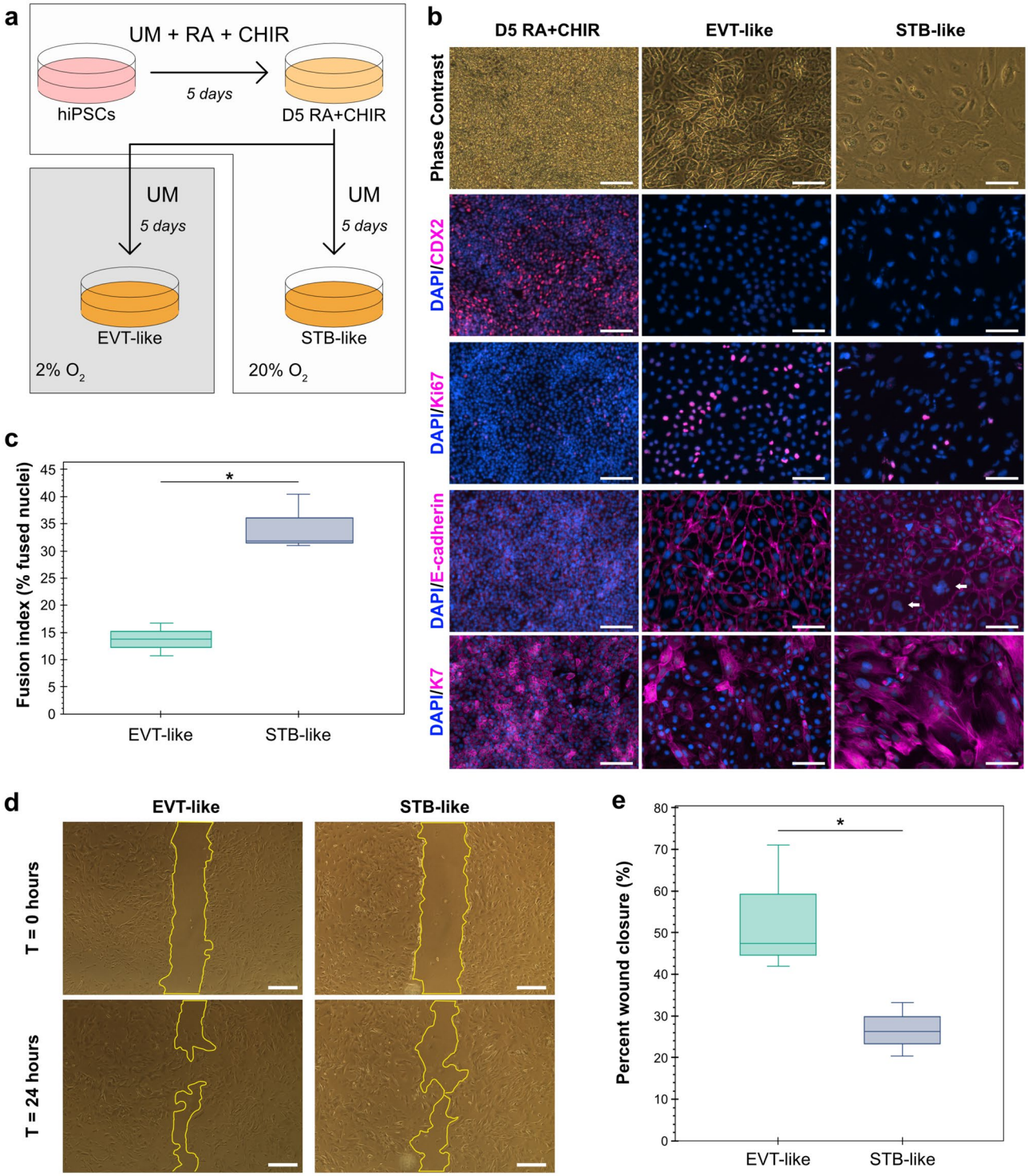

Figure 5. RA + CHIR-treated cells can be differentiated to EVT-like and STB-like cells. (**a**) Schematic diagram depicting the differentiation strategy. (**b**) Phase contrast and immunocytochemistry images after 5 days of differentiation in UM containing RA + CHIR (D5 RA + CHIR) or after subculture and an additional 5 days in UM with hypoxia (EVT-like) or normoxia (STB-like). Scale bar indicates 100 µm. White arrows denote sites of multinucleation. (**c**) Quantification of the fusion index in EVT-like and STB-like cells. (**d**) Phase contrast images immediately after scratch and 24 h after scratch in EVT-like and STB-like cells. Scale bar indicates 500 µm. Yellow outlines denote leading edge of cells. (**e**) Quantification of the percent of wound closure in EVT-like and STB-like cells. *$p \leq 0.05$ based on t-test of three independent experimental replicates. Data are presented as mean ± SD of three independent experiments.

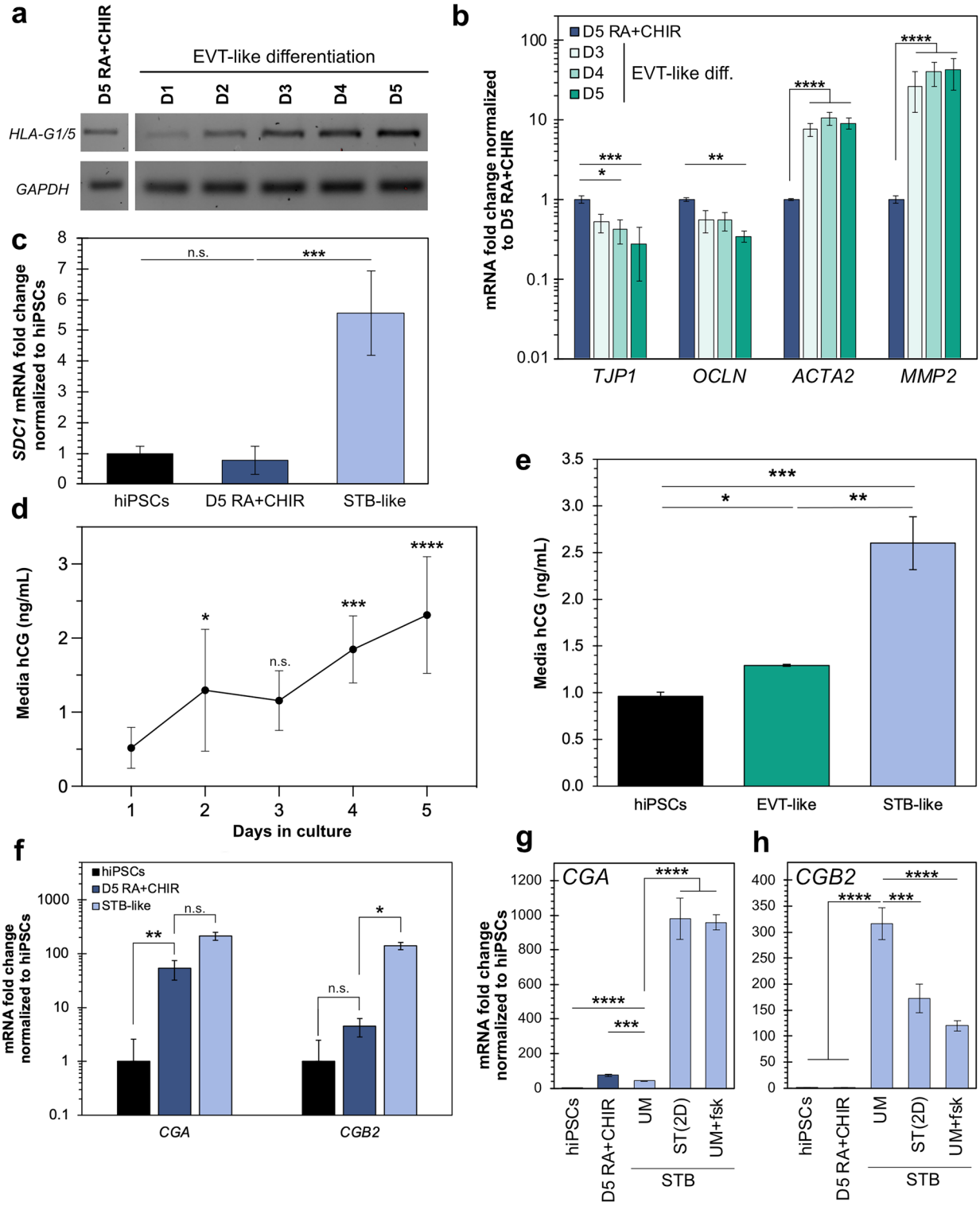

Figure 6. EVT-like and STB-like cells derived from day 5 RA + CHIR-treated cells show functional phenotypes. (**a**) RT-PCR of cells after 5 days of RA + CHIR or after sub-culture and maintenance in hypoxia for an additional 1, 2, 3, 4, or 5 days (D1-D5). Original gel is presented in Fig. S14. (**b**) qRT-PCR analysis of cells during days 3, 4, and 5 (D3-D5) in hypoxia treatment compared to day 5 RA + CHIR. (**c**) qRT-PCR analysis of *SDC1* in hiPSCs, day 5 RA + CHIR cells, and STB-like cells normalized to hiPSCs. *GAPDH* was used as a reference gene. (**d**) hCG media concentration determined by ELISA on conditioned media from STB-like differentiated cells treated in normoxia for 1–5 days. Error bars indicate SEM of 3 independent replicates. Significance is determined based on comparison to day 1. (**e**) hCG concentration in media conditioned with hiPSCs, EVT-like cells, and STB-like cells. (**f**) qRT-PCR analysis of *CGA* and *CGB2* in hiPSCs, day 5 RA + CHIR cells, and STB-like cells normalized to hiPSCs, *GAPDH* was used as a reference gene. (**g**,**h**) qRT-PCR analysis of *CGA* (**g**) and *CGB2* (**h**) in hiPSCs, day 5 RA + CHIR cells, STB-like cells (UM), ST(2D)-treated cells, and UM + forskolin-treated (UM + fsk) cells. Transcript levels are shown relative to *GAPDH* expression and normalized to hiPSC expression. Data are presented as mean ± SD of three independent replicates unless otherwise specified. n.s. = not significant, *$p \le 0.05$, **$p \le 0.01$, ***$p \le 0.001$, ****$p \le 0.0001$ based on ANOVA of three independent experimental replicates.

genes *MMP2* and *ACTA2* were more than tenfold upregulated in hypoxic conditions when compared to day 5 RA + CHIR-treated cells, demonstrating evidence of EMT in hypoxia-treated cells (Fig. 6b).

STB-like cells show significant upregulation of syndecan 1 (*SDC1*), which is highly expressed in human STB (Fig. 6c). We also quantified the level of hCG in the conditioned media and observed a significant increase during the differentiation, with day 5 levels of 2.3 ± 0.8 ng/mL (Fig. 6d). Day 5 levels in STB-like cells were significantly higher than levels of hCG observed from conditioned media of hiPSCs and EVT-like cells (Fig. 6e). Though we were consistently able to detect hCG in conditioned media, the detected value was low and often varied significantly across independent differentiations. For this reason, we also quantified hCG mRNA transcript subunits in STB-like cells. Though the levels of *CGA* were only slightly upregulated, across multiple hiPSC lines we observed more than 20-fold upregulation of *CGB2* in STB-like cells compared to day 5 RA + CHIR treated cells (Figs. 6f, S13).

Given the low protein level expression of hCG and only modest upregulation of *hCG* mRNA subunits in our cells, we tested whether another STB specification protocol applied to our day 5 RA + CHIR treated cells could improve the differentiation[3]. We discovered that ST(2D) medium increased the expression of *CGA* over 20-fold when compared to UM alone, while expression of *CGB*2 remained high (Fig. 6g,h). Modification of our original protocol for STB-like cells to replicate some features of the ST(2D) method (i.e., inclusion of 2 µM forskolin to the UM and media change only on day 3) showed similar expression of *CGA* and *CGB2* as the ST(2D) protocol (Fig. 6g,h).

Furthermore, we analyzed the various STB differentiation protocols for their effect on expression of a panel of genes associated with STB differentiation (Fig. S17). We quantified the expression of *ERW-1* and *ERVFRD-1* (Syncytins 1 and 2, respectively, necessary for the multinucleated cell phenotype observed in STB cells), *TEAD4* (trophoblast stem cell transcription factor), and *GCM1* (transcription factor highly expressed in STB and EVT cells), which have previously been assessed in stem cell-derived models of STB, as well as some genes that have not previously been analyzed in these models: *OVOL1* (transcription factor promoting STB differentiation) and *HSD11B2* (glucocorticoid enzyme)[37–39]. *ERW-1*, *ERVFRD-1*, *OVOL1*, and *GCM1* were all upregulated to varying degrees (1.5-fold to tenfold) in the tested STB differentiations (Fig. S17). Expression of *TEAD4* decreased during the differentiation, as expected (Fig. S17). However, *HSD11B2* (glucocorticoid enzyme) was not upregulated in any tested condition (Fig. S17). These data demonstrate that modifications to the subtype differentiation method can improve relevant transcript expression, but also that further optimization may be needed to enhance differentiation toward STB-like cells for studies of this cell population.

Discussion

Development of a simple, relevant model of the placenta will lead to improved understanding of the formation of trophoblast cells and their subsequent subtype differentiation. Knowledge of this critical process has largely been hindered by regulations understandably protecting early fetal tissue, but stem cell-derived models provide an alternative platform to study these mechanisms. The initial BMP-4-induced models have been debated in the field; specifically they have been critiqued for low expression of *ELF5* compared to primary trophoblast cells and lack of HLA-G expression[16]. Recent modifications to the initial BMP-4-treated stem cell models have rescued some of these key features, but current approaches (either with or without BMP-4) to derive functional placental cells can take weeks to generate or involve treatment with multiple interacting small molecules and growth factors[17,18]. In this study, we assessed the trophoblast-like cells for the four criteria outlined by experts in the field for high-fidelity models of trophoblast cells: expression of (1) *ELF5*; (2) C19MC miRNAs; (3) *KRT7*, *TFAP2C*, and *GATA3*; and (4) *HLA-G*[16].

The promoter region of ELF5 is known to be hypomethylated in placental cells and hypermethylated in embryonic stem cells[16]. Though the relationship between methylation status and expression of ELF5 in human trophoblast cells remains unclear, ELF5 expression is restricted to cytotrophoblast cells in the human placenta[40]. While previous stem cell-derived trophoblast cell models were critiqued for insufficient hypomethylation of the ELF5 promoter and low *ELF5* expression, the RA + CHIR-treated cells expressed mRNA transcript levels of *ELF5* comparable to day 8 primary TE. Of the stem cell-derived trophoblast cell models compared in this work, day 5 RA + CHIR-treated cells had the highest *ELF5* expression, but only the primed TSCs had significantly lower *ELF5* expression than primary TE.

Expression of C19MC miRNAs is a key feature of human trophoblast cells[28]. Significantly lower expression of C19MC miRNAs in stem cell-derived trophoblast cell models compared to primary cells has recently been an area of concern, though recent improvements using naïve hPSCs have rescued C19MC miRNA expression[29,41,42]. Most studies thus far have not reported analysis of C19MC miRNA expression in their cells[13,17,18,22], but previous studies that have quantified C19MC miRNA expression demonstrated primed hPSC-derived, BMP-4-induced trophoblast cell models had up to 4000-fold lower expression when compared to choriocarcinoma lines[16,29]. Conversely, in our analysis of the RA + CHIR-treated cells, C19MC miRNAs *525-3p* and *526b-3p* showed similar expression and miRNAs *517a* and *517b* showed only tenfold lower expression than BeWo cells, indicating improved agreement with primary cells.

RA + CHIR-treated cells also express high levels of *KRT7*, *TFAP2C*, and *GATA3* transcripts and robustly express both keratin 7 and GATA3 at the protein level. Finally, we demonstrate expression of *HLA-G* transcripts in both day 5 RA + CHIR-treated cells and in EVT-like cells cultured in hypoxia. *HLA-G1/5* expression was inhibited in cells cultured in normoxia, as expected[43,44]. Overall, our simple model fulfilled all established criteria and generated multipotent trophoblast-like cells with quality similar to other stem cell-derived models in just 5 days of treatment and with only two small-molecule inducers.

Recent studies of trophoblast cell models derived from primed hPSCs have demonstrated similarity to amnion-like cells as opposed to trophoblast cells[45,46]. Amnion cells are epithelial cells that form the extraembryonic tissue

known as the amniotic sac, which functions to mechanically protect the developing embryo and provide key signaling cues[46]. Amnion cells are known to express key trophoblast markers including *GATA3*, *CDX2*, and *TFAP2C* but they also express other markers including vimentin (*VIM*), insulin gene enhancer protein (*ISL1*), and cadherin 10 (*CDH10*) that are not known to be expressed in human trophoblast cells[45]. Cells treated with RA and CHIR for five days express key trophoblast cell markers, but do not express *VIM* or *CDH10* which were shown to be highly expressed in TSCs derived from primed cells (Fig. S12). They do however show moderate transcript level expression of *ISL1*, which more closely resembles the expression pattern of hPSC-derived TESCs (Fig. S12). In studies that have concluded primed hPSCs are only capable of differentiating into amnion cells, only BMP-4 induced differentiations have been analyzed[19,45,46]. Furthermore, there still remains debate in the field regarding the amnion identity of BMP-4-treated primed hPSCs[41]. Our method does not use BMP-4, and RA + CHIR-treated cells exhibit some key transcriptional differences compared to BMP-4-derived primed TSCs (Figs. 4b,e, S7, S8). Therefore, further investigation is necessary to understand the potential of primed hPSCs to differentiate towards extraembryonic tissues formed during the peri-implantation period.

RA has been used ubiquitously in stem cell differentiations toward many lineages[47–52]. Furthermore, RA has been implicated in extraembryonic tissue development and germ cell differentiation[20,53]. Jagtap and colleagues demonstrate upregulation of both trophectoderm and primitive endoderm markers following 7-day treatment with 5 μM RA[20]. In another study, Cheng and colleagues show 12 days of treatment with 2 μM RA in combination with 8 μM CHIR initiated differentiation toward primordial germ cells[53]. Our RNA-seq data demonstrate expression consistent with primary TE and inconsistent with germ-layer specific cells, primitive endoderm cells, or primordial germ cells during the 5-day differentiation with 1 μM RA and 8 μM CHIR, indicating there are likely strong concentration- and time-dependent effects of RA on cell fate during differentiation. Previous research showed RA treatment of stem cells agonized TGF-β signaling via upregulation of BMP-4[20], which is consistent with the results of our upstream analysis (Table S3); these results could help explain why RA, as used in this work, obviates the need for BMP-4 in producing trophoblast cells.

Other stem cell-derived trophoblast cell models have demonstrated self-renewal of their populations[17,18,22,29]. We have concluded that though RA + CHIR is capable of inducing the trophoblast cell state, maintenance of these cells in RA + CHIR-containing media does not promote proliferation. However, other media formulations for maintenance of both primary and stem cell-derived trophoblast cells should be explored to determine if RA + CHIR induces cells that can be stably maintained in culture prior to subtype specification.

We also demonstrated the capacity for RA + CHIR-treated cells to be differentiated into cells with features of EVT and STB cells. Our EVT-like cells express the membrane-bound isoform of HLA-G (*HLA-G1/5*) at the mRNA level, show transcriptional evidence of EMT, and are more migratory than the STB-like cells derived in parallel. Our STB-like cells demonstrate multinucleation and expression of STB-related genes *SDC1*, *CGA* , and *CGB2*. Though STB-like cells derived from RA + CHIR-treated cells had some features indicative of STB cells, we obtained only modest and variable expression of hCG, and some analyzed genes were not upregulated in any STB-inducing condition attempted (i.e., *HSD11B2*). To our knowledge, no other studies have reported *HSD11B2* or *OVOL1* expression in stem cell-derived STB-like cells. However, it has been shown that STB-like cells derived from BMP-4 treatment can secrete 20- to 30-fold more hCG following differentiation whereas we saw a modest threefold increase[22,29,54], indicating an opportunity for further optimization of differentiation toward EVT-like and STB-like cells from RA + CHIR-induced trophoblast-like cells. Despite these shortcomings, RA + CHIR-treated cells have the potential for differentiation into cells with functional characteristics of human placental cells.

The RA + CHIR-treated cells developed in this work represent a rapid, robust platform for generation of trophoblast-like cells that meet or exceed all trophectoderm model benchmarks set by the current BMP-4-derived models. Additionally, the use of small molecules as opposed to growth factors minimizes costs and prevents variability in output, improvements critical for performing experiments at scale. This RA + CHIR-treated, stem cell-derived trophoblast-like cell model represents a powerful in vitro tool to aid in the understanding of placentation during development and disease.

Methods

Stem cell culture

Human induced pluripotent stem cell lines iPS(IMR90)-4 (WiCell), ACS-1024 (ATCC), and UMN PCBC-16iPS (a kind gift from the Dutton Lab, University of Minnesota Stem Cell Institute, generated as previously described[55]) were used in this study. Stem cells were maintained on hESC-qualified Matrigel (Corning) or Stem Cell Qualified, Reduced Growth Factor Cultrex (R&D Systems) in TeSR-E8 or mTeSR Plus (STEMCELL Technologies) in a 37 °C incubator with 5% CO_2. Medium was changed daily. Stem cells were passaged every 5–6 days at 70% confluence using ReLeSR (STEMCELL Technologies) at a split ratio of 1:18 as the manufacturer describes.

All stem cell lines were banked in 1 mL mFreSR (STEMCELL Technologies) as the manufacturer recommends at 1 well/vial and stored in liquid nitrogen. For thawing, frozen cell stocks were swirled in a 37 °C water bath and then added dropwise to 11 mL of maintenance medium. Cells were spun down at 200 × g for 5 min, resuspended in growth medium containing 10 μM ROCK inhibitor (Y-27632, STEMCELL Technologies), and distributed into 3 wells of an ECM-coated 6 well plate (Corning). Medium (without ROCK inhibitor) was changed 24 h later.

Appropriate cell morphology and sterility were assessed daily by visual inspection. When necessary, areas of spontaneous differentiation were marked and removed using a 200 μL pipette tip. In addition to morphology, markers of the undifferentiated state were assessed via flow cytometry and qRT-PCR periodically during stem cell maintenance. Cells were tested monthly for mycoplasma contamination using MycoAlert (Lonza) and were tested prior to banking for normal karyotype using G-banding analysis (7–10 metaphases analyzed). Only cells within 10 passages from thaw were used in experiments.

Differentiation to trophoblast cells

For differentiation, 70% confluent stem cells were rinsed with DPBS (Gibco) and pre-warmed Accutase (STEMCELL Technologies) was added to the wells. Cells were then placed at 37 °C for 5–7 min, after which they were added to an equal volume of fresh medium and spun down at 200xg for 5 min. The cells were then resuspended and seeded on Matrigel- or Cultrex-coated plates at 6000 cells/cm^2 in TeSR-E8 or mTeSR Plus with 5 μM ROCK inhibitor. Cells were maintained in E8 or mTeSR Plus for two more days, and then the medium was changed to unconditioned medium (UM): DMEM/F12 with 20% Knockout serum replacement (KOSR), MEM non-essential amino acids (1x), GlutaMAX (1x, Gibco), and 0.1 mM β-mercaptoethanol (Sigma), containing 1 μM retinoic acid (RA, Sigma) and 8 μM CHIR 99021 (CHIR, Tocris). Where denoted, IWP2 (Tocris) was added during the differentiation. Cell culture medium was changed daily for five days.

For differentiation to STB-like and EVT-like subtypes, cells maintained in UM with RA and CHIR were subcultured using Accutase as described above. Cells were seeded at 20,000 cells/cm^2 on Matrigel-coated or Cultrex-coated plates in UM with 5 μM ROCK inhibitor for 24 h. For STB-like specification, cells were maintained in UM with 20% O_2 for five days, and for EVT-like specification, cells were maintained in UM under hypoxic conditions (1–2% O_2) using a hypoxia incubator chamber (STEMCELL Technologies) placed inside a 37 °C incubator for five days. Medium was changed daily. Subculture seeding densities for trophoblast subtype differentiations required optimization (20,000–30,000 cells/cm^2 range) as passage number increased.

Where denoted, cells maintained in UM with RA and CHIR for 5 days were subcultured in ST(2D) medium and cultured as previously described[3]. Briefly, cells were seeded at 20,000 cells/cm^2 in ST(2D) medium (DMEM/F12, 0.1 mM 2-mercaptoethanol, 0.5% penicillin–streptomycin (Gibco), 0.3% BSA (Sigma), 1% ITS-X supplement (Gibco), 2.5 μM ROCK inhibitor, 2 μM forskolin (Tocris), and 4% KOSR). Medium was changed to ST(2D) without ROCK inhibitor on day three, and cells were collected for analysis on day six. Where denoted, cells maintained in UM with RA and CHIR for 5 days were subcultured at 20,000 cells/cm^2 into UM with 2 μM forskolin and 2.5 μM ROCK inhibitor. Medium was changed to UM with 2 μM forskolin on day three, and cells were collected for analysis on day six.

Immunostaining

For immunocytochemistry analysis, cells were rinsed 2X with PBS and then fixed for 10 min with 4% paraformaldehyde (PFA, Polysciences) at room temperature. Following 3X 5-min washes in PBS, cells were blocked in PBSGT—PBS with 5% goat serum and 0.3% Triton-X-100 (Sigma)—for 1 h. Primary antibodies (Table S5) were diluted in PBSGT and incubated overnight at 4 °C. Cells were washed 3X in PBST for 15 min, and then secondary antibodies (Table S6) in PBSGT were added and incubated for 1 h at room temperature. Following a 10 min PBS wash, cells were incubated with 4′,6-diamidino-2-phenylindole, dihydrochloride (DAPI, Life Technologies) for 10 min. Another 10 min PBS wash was performed before the cells were imaged on an EVOS FL Auto fluorescence microscope (Thermo Fisher Scientific).

Flow cytometry

Cells were rinsed 2X with PBS and pre-warmed Accutase was added. The well plates were incubated at 37 °C for 5–7 min. Cells were spun down at 200 × g for 5 min, followed by resuspension in 1 mL 4% PFA for 10 min at room temperature. PFA was removed by a spin at 200xg for 5 min, and cells were then incubated with ice-cold 90% methanol (Sigma) for 30 min on ice or overnight at – 20 °C. Cells were distributed to 200,000 cells per tube and vortexed with 3 mL FACS buffer (PBS + 2% FBS (Gibco) + 0.1% Triton X-100). FACS buffer was removed by a spin at 240 × g for 5 min. For primary antibody incubation, 50 μL FACS buffer containing primary antibody (Table S5) was added and incubated overnight at 4 °C. Cells were vortexed with 3 mL FACS buffer and spun down. Then, 50 μL secondary antibody (Table S6) in FACS buffer was added and incubated for 30 min at room temperature. Cells were washed with 3 mL FACS buffer, spun down, and resuspended in 300 μL FACS buffer.

Analysis was performed on a BD LSR II H4710. At least 50,000 cells/sample were collected, and analysis was performed in FlowJo (BD). Expression values were plotted on a biexponential axis. Plots shown are representative of a single experiment, but median, standard deviation, and interquartile range (IQR) were calculated from three independent replicates. As a measure of spread, IQR was calculated from the single-cell fluorescence data as quartile 3 (Q3, upper median)—quartile 1 (Q1, lower median). Data are presented as median plus or minus the standard deviation.

Enzyme-linked immunosorbent assays (ELISA)

Medium conditioned on STB-like cells was collected and immediately stored at – 80 °C prior to analysis. Levels of hCG were quantified in duplicate using the hCG ELISA Kit (Abnova) as the manufacturer recommends. Optical density (OD) readings were performed on a BioTek plate reader at 450 nm with the first calibrator set to zero.

qRT-PCR and RT-PCR

Cell pellets were collected and lysed using QiaShredder columns (Qiagen). RNA was isolated using the RNeasy Mini Kit (Qiagen) as the manufacturer recommends, including incubation with DNase I (RNAse-free DNase Set, Qiagen). Collected RNA was quantified using a NanoDrop (Thermo Fisher Scientific). Reverse transcription was performed on 1000 ng RNA using the Omniscript RT Kit (Qiagen). RNA with Oligo(dT)$_{20}$ primers (Invitrogen) or miRNA-specific RT primers (Table S7) was denatured for 5 min at 65°C prior to addition of the remaining elements and incubation at 37 °C for 1 h. Quantitative real time PCR (qRT-PCR) was performed using iTaq Universal SYBR Green Supermix (Bio-Rad) as the manufacturer recommends. Primers (Tables S7, S8) were added at 250 nM each (forward and reverse). Analysis was performed on a Bio-Rad CFX Connect Real-Time

PCR system with *GAPDH* used as a reference gene. The ΔΔCt method was used to calculate fold changes and propagate error.

Reverse transcription PCR (RT-PCR) was performed identically as above through the reverse transcription step to generate cDNA. GoTaq Master Mix (Promega) was used for RT-PCR per the instructions from the manufacturer. Primers (Table S8) were added at 250 nM each. RT-PCR products were visualized on a 2% agarose (Invitrogen) gel containing SYBR Safe (Thermo Fisher Scientific) after electrophoresis at 75 V for 100 min. Gels were imaged using a ChemiDoc Touch Imaging System (Bio-Rad).

For BeWo cell transcriptional analyses, a frozen cell stock was kindly gifted by Dr. Sarah Wernimont (University of Minnesota Medical School). The vial was thawed in a 37 °C water bath and spun down at 200 × g for 5 min to pellet the cells. Cell lysis, RNA extraction, and qRT-PCR steps were performed as described above.

RNA sequencing

RNA from two independent experiments was collected from cell pellets as previously described above using QiaShredder columns and the RNeasy Mini Kit (Qiagen). The sequencing libraries were prepared using TruSeq Stranded mRNA (Illumina), and paired-end sequencing was performed in one lane of NovaSeq 6000 SPrime (Illumina) with a read length of 50 bp (yielding ~ 40 M reads per sample). Low-quality sequences and adaptors were removed using Trimmomatic, and sequences were then mapped to the human reference genome (GRCh38.91) using STAR. Fragments per kilobase of transcript per million mapped reads (FPKM) files were obtained using cufflinks, and counts per million (CPM) files were obtained by using the htseq package in Python. FPKM files were converted to transcripts per million (TPM) files for subsequent heatmaps and clustering analyses.

Correlation and gene expression analysis

To compare primary cells and those differentiated using BMP-4 to our samples, FPKM files GSE109555, GSE138688, and GSE137295 were obtained from the GEO database[17,18,30]. GSE109555 contained single-cell data from cells identified as human epiblast (EPI), primitive endoderm (PE), and trophectoderm (TE) from 65 different embryos. Single-cell data from each day and cell type were pooled and averaged to compare to batch RNA-seq datasets (only samples with > 20 cells/condition were included). Lowly expressed genes were set to an arbitrarily low $\log_2$(TPM) value of − 20 for numerical analyses. All four datasets were normalized using quantile normalization, and batch correction was performed using the ComBat package[56]. Plot generation and linear dimension reduction operations were carried out in R (R-4.3.2, https://cran.r-project.org/). Heatmaps were generated using the ComplexHeatmap package (2.20.0, https://github.com/jokergoo/ComplexHeatmap/) available from Bioconductor.

Differential gene expression (DGE) analysis

CPM files for hTSCs, hTESCs, CT29, and CT30 cells were obtained from GSE138762[17]. This dataset was merged with CPM files obtained from RA + CHIR-treated cells prior to batch correction using ComBat-seq[57]. Genes with CPM values less than 100 were removed, which reduced the number of genes from 57,750 to 4,085, and then the counts files were normalized based on total expression. Tagwise dispersions were estimated and then DGE was performed using edgeR[58–61]. Benjamini and Hochberg's algorithm was used to control the false discovery rate (FDR). Significantly differentially expressed genes were defined as having a fold change greater than 4 (either up or down regulation) and an FDR less than 0.01. Analyses and volcano plot formation processes were carried out in R (R 4.3.2, https://cran.r-project.org/). Pathway analyses and upstream regulator analyses were performed using the Ingenuity Pathway Analysis package (IPA, Qiagen).

Fusion index

EVT-like and STB-like cells were differentiated as previously described above. Immunocytochemistry for E-cadherin was performed as previously described on STB-like and EVT-like cells. Images were analyzed in ImageJ to obtain the number of total cells and the number of cells residing within syncytia. Fusion index was calculated as shown in Eq. (1). Three images per replicate were quantified (technical replicates), and three independent experiments were performed for each condition. Data are presented as mean plus or minus the standard deviation.

$$\frac{\#\ nuclei\ in\ syncytia}{total\ \#\ of\ nuclei\ in\ field\ of\ view} x100\% \quad (1)$$

Wound healing assay

Following EVT-like and STB-like cell differentiation as previously described, a 200 µL pipette tip was used to create a scratch in three separate areas in the culture dish. Cells were rinsed twice with DPBS to remove any scraped cells and then imaged using an EVOS FL Auto microscope. Following incubation for 24 h, cells were imaged again in the same location. Percent of wound closure values were determined using ImageJ to quantify the cell-free surface area at 24 h normalized to the cell-free surface area at 0 h. Three regions were tracked for each replicate with three independent experiments performed for each condition, and data are presented as mean plus or minus the standard deviation.

Equipment and settings

For microscopy images, all images were captured on an EVOS FL Auto fluorescence microscope using EVOS FL Auto software in 8-bit TIFF format with a size of 3.7 mega pixels (2506 × 1476 pixels). Intensity of each laser was adjusted to background levels in negative control conditions and below saturation for high expression conditions and then kept consistent throughout acquisition for an experiment. Only images from a single experiment (single laser intensity) are shown together. Contrast was set to 33.3 and saturation was set to 57. DAPI was imaged using a DAPI light cube (357/44 nm excitation, 447/60 nm emission), AF488 was imaged using a GFP light cube (482/25 nm excitation, 524/24 nm emission), AF594 was imaged using a Texas Red light cube (595/29 nm excitation, 628/32 nm emission), and AF647 was imaged using a Cy5 light cube (628/40 nm excitation, 692/40 nm emission).

All gel images were captured on a ChemiDoc Touch Imaging System with a Chemi/UV/Stain-free sample tray using a UV trans illuminator (590/110 filter). Exposures were set manually for each gel and kept between 3 and 5 s to prevent saturation of image bands. Image colors were inverted to make the background light and the bands dark. Images were saved in TIFF format with a size of 8.2 mega pixels (3202 × 2561 pixels). Only bands from the same gel are shown together in figure subpanels. Gel images were cropped for clarity, but original gel images are presented in the supplement (Figs. S4, S14–S16).

Statistical analyses

Experiments contained at least 3 independent replicates each with 3 technical replicates unless otherwise specified, and a representative condition was displayed where applicable. Statistical analyses were performed in GraphPad Prism software. P-values were determined using t-test or ANOVA with Dunnett's multiple comparison analysis and are noted in the figure legends were appropriate.

Data availability

The datasets used and/or analyzed during the current study are available from the corresponding author on reasonable request. RNA-sequencing data generated in this manuscript will be publicly available from the Gene Expression Omnibus (GSE232692) from August 31, 2024.

Received: 31 January 2024; Accepted: 30 July 2024
Published online: 06 August 2024

References

1. Latos, P. A. & Hemberger, M. From the stem of the placental tree: Trophoblast stem cells and their progeny. *Dev. Camb.* **143**, 3650–3660 (2016).
2. Knöfler, M. *et al.* Human placenta and trophoblast development: Key molecular mechanisms and model systems. *Cell. Mol. Life Sci.* **76**, 3479–3496 (2019).
3. Okae, H. *et al.* Derivation of human trophoblast stem cells. *Cell Stem Cell* **22**, 50-63.e6 (2018).
4. Bilban, M. *et al.* Trophoblast invasion: Assessment of cellular models using gene expression signatures. *Placenta* **31**, 989–996 (2010).
5. Tan, J. P., Liu, X. & Polo, J. M. Establishment of human induced trophoblast stem cells via reprogramming of fibroblasts. *Nat. Protoc.* **17**, 2739–2759 (2022).
6. Castel, G. & David, L. Induction of human trophoblast stem cells. *Nat. Protoc.* **17**, 2760–2783 (2022).
7. Blakeley, P. *et al.* Defining the three cell lineages of the human blastocyst by single-cell RNA-seq. *Development* **142**, 3613 (2015).
8. Molè, M. A., Weberling, A. & Zernicka-Goetz, M. *Comparative analysis of human and mouse development: From zygote to pre-gastrulation*. *Current Topics in Developmental Biology* vol. 136 (Elsevier Inc., 2020).
9. Fogarty, N. M. E. *et al.* Genome editing reveals a role for OCT4 in human embryogenesis. *Nature* **550**, 67–73 (2017).
10. Kuckenberg, P. *et al.* The transcription factor TCFAP2C/AP-2γ Cooperates with CDX2 to maintain trophectoderm formation. *Mol. Cell. Biol.* **30**, 3310–3320 (2010).
11. Ralston, A. *et al.* Gata3 regulates trophoblast development downstream of Tead4 and in parallel to Cdx2. *Development* **137**, 395–403 (2010).
12. Xu, R. H. *et al.* BMP4 initiates human embryonic stem cell differentiation to trophoblast. *Nat. Biotechnol.* **20**, 1261–1264 (2002).
13. Horii, M., Bui, T., Touma, O., Cho, H. Y. & Parast, M. M. An improved two-step protocol for trophoblast differentiation of human pluripotent stem cells. *Curr. Protoc. Stem Cell Biol.* **50** (2019).
14. Cambuli, F. *et al.* Epigenetic memory of the first cell fate decision prevents complete ES cell reprogramming into trophoblast. *Nat. Commun.* **5**, 1–16 (2014).
15. Roberts, R. M. *et al.* Differentiation of trophoblast cells from human embryonic stem cells: To be or not to be? *Reproduction* **147** (2014).
16. Lee, C. Q. E. *et al.* What is trophoblast? A combination of criteria define human first-trimester trophoblast. *Stem Cell Rep.* **6**, 257–272 (2016).
17. Mischler, A. *et al.* Two distinct trophectoderm lineage stem cells from human pluripotent stem cells. *J. Biol. Chem.* **296** (2021).
18. Dong, C. *et al.* Derivation of trophoblast stem cells from naïve human pluripotent stem cells. *eLife* **9**, 1–26 (2020).
19. Guo, G. *et al.* Human naive epiblast cells possess unrestricted lineage potential. *Cell Stem Cell* **28**, 1040-1056.e6 (2021).
20. Jagtap, S. *et al.* All-trans retinoic acid and basic fibroblast growth factor synergistically direct pluripotent human embryonic stem cells to extraembryonic lineages. *Stem Cell Res.* **10**, 228–240 (2013).
21. Knöfler, M. & Pollheimer, J. Human placental trophoblast invasion and differentiation: A particular focus on Wnt signaling. *Front. Genet.* **4**, 190 (2013).
22. Horii, M. *et al.* Human pluripotent stem cells as a model of trophoblast differentiation in both normal development and disease. *Proc. Natl. Acad. Sci. USA* **113**, E3882–E3891 (2016).
23. Niakan, K. K. & Eggan, K. Analysis of human embryos from zygote to blastocyst reveals distinct gene expression patterns relative to the mouse. *Dev. Biol.* **375**, 54–64 (2013).
24. Wang, C. C., Jamal, L. & Janes, K. A. Normal morphogenesis of epithelial tissues and progression of epithelial tumors. *Wiley Interdiscip. Rev. Syst. Biol. Med.* **4**, 51–78 (2012).
25. Li, Z., Kurosawa, O. & Iwata, H. Establishment of human trophoblast stem cells from human induced pluripotent stem cell-derived cystic cells under micromesh culture. *Stem Cell Res. Ther.* **10** (2019).

26. Krendl, C. *et al.* GATA2/3-TFAP2A/C transcription factor network couples human pluripotent stem cell differentiation to trophectoderm with repression of pluripotency. *Proc. Natl. Acad. Sci. USA* **114**, E9579–E9588 (2017).
27. Blanchon, L. *et al.* Activation of the human pregnancy-specific glycoprotein PSG-5 promoter by KLF4 and Sp1. *Biochem. Biophys. Res. Commun.* **343**, 745–753 (2006).
28. Donker, R. B. *et al.* The expression profile of C19MC microRNAs in primary human trophoblast cells and exosomes. *Mol. Hum. Reprod.* **18**, 417–424 (2012).
29. Soncin, F. *et al.* Derivation of functional trophoblast stem cells from primed human pluripotent stem cells. *Stem Cell Rep.* **17**, 1303–1317 (2022).
30. Zhou, F. *et al.* Reconstituting the transcriptome and DNA methylome landscapes of human implantation. *Nature* **572**, 660–664 (2019).
31. Chang, C. W., Wakeland, A. K. & Parast, M. M. Trophoblast lineage specification, differentiation and their regulation by oxygen tension. *J. Endocrinol.* **236**, R43–R56 (2018).
32. Hutchins, A. P. *et al.* Models of global gene expression define major domains of cell type and tissue identity. *Nucleic Acids Res.* **45**, 2354–2367 (2017).
33. Du, R. *et al.* Hypoxia-induced down-regulation of microRNA-34a promotes EMT by targeting the Notch signaling pathway in tubular epithelial cells. *PLoS ONE* **7**, e30771 (2012).
34. Haider, S. *et al.* Self-renewing trophoblast organoids recapitulate the developmental program of the early human placenta. *Stem Cell Rep.* **11**, 537–551 (2018).
35. Apps, R. *et al.* Human leucocyte antigen (HLA) expression of primary trophoblast cells and placental cell lines, determined using single antigen beads to characterize allotype specificities of anti-HLA antibodies. *Immunology* **127**, 26–39 (2009).
36. Davies, E. *et al.* Epithelial-mesenchymal transition during extravillous trophoblast differentiation. *Cell Adhes. Migr.* **10**, 310–321 (2016).
37. Papuchova, H. & Latos, P. A. Transcription factor networks in trophoblast development. *Cell. Mol. Life Sci.* **79**, 337 (2022).
38. Jeyarajah, M. J. *et al.* The multifaceted role of GCM1 during trophoblast differentiation in the human placenta. *Proc. Natl. Acad. Sci. U. S. A.* **119**, (2022).
39. Green, B. B. *et al.* The role of placental 11-beta hydroxysteroid dehydrogenase type 1 and type 2 methylation on gene expression and infant birth weight. *Biol. Reprod.* **92**, 149–150 (2015).
40. Hemberger, M., Udayashankar, R., Tesar, P., Moore, H. & Burton, G. J. ELF5-enforced transcriptional networks define an epigenetically regulated trophoblast stem cell compartment in the human placenta. *Hum. Mol. Genet.* **19**, 2456–2467 (2010).
41. Kobayashi, N. *et al.* The microRNA cluster C19MC confers differentiation potential into trophoblast lineages upon human pluripotent stem cells. *Nat. Commun.* **13**, 1–14 (2022).
42. Karvas, R. M. *et al.* Stem-cell-derived trophoblast organoids model human placental development and susceptibility to emerging pathogens. *Cell Stem Cell* **29**, 810-825.e8 (2022).
43. Alsat, E. *et al.* Hypoxia impairs cell fusion and differentiation process in human cytotrophoblast, in vitro. *J. Cell. Physiol.* **168**, 346–353 (1996).
44. Nelson, D. M., Johnson, R. D., Smith, S. D., Anteby, E. Y. & Sadovsky, Y. Hypoxia limits differentiation and up-regulates expression and activity of prostaglandin H synthase 2 in cultured trophoblast from term human placenta. *Am. J. Obstet. Gynecol.* **180**, 896–902 (1999).
45. Io, S. *et al.* Capturing human trophoblast development with naive pluripotent stem cells in vitro. *Cell Stem Cell* **28**, 1023-1039.e13 (2021).
46. Rostovskaya, M., Andrews, S., Reik, W. & Rugg-Gunn, P. J. Amniogenesis occurs in two independent waves in primates. *Cell Stem Cell* **29**, 744-759.e6 (2022).
47. Lippmann, E. S. *et al.* Deterministic HOX patterning in human pluripotent stem cell-derived neuroectoderm. *Stem Cell Rep.* **4**, 632–644 (2015).
48. Wobus, A. M. *et al.* Retinoic acid accelerates embryonic stem cell-derived cardiac differentiation and enhances development of ventricular cardiomyocytes. *J. Mol. Cell. Cardiol.* **29**, 1525–1539 (1997).
49. Lippmann, E. S., Al-Ahmad, A., Azarin, S. M., Palecek, S. P. & Shusta, E. V. A retinoic acid-enhanced, multicellular human blood-brain barrier model derived from stem cell sources. *Sci. Rep.* **4**, 1–10 (2014).
50. Gudas, L. J. & Wagner, J. A. Retinoids regulate stem cell differentiation. *J. Cell. Physiol.* **226**, 322–330 (2011).
51. Cabezas-Wallscheid, N. *et al.* Vitamin A-retinoic acid signaling regulates hematopoietic stem cell dormancy. *Cell* **169**, 807-823. e19 (2017).
52. Tang, X. H. & Gudas, L. J. Retinoids, retinoic acid receptors, and cancer. *Annu. Rev. Pathol. Mech. Dis.* **6**, 345–364 (2011).
53. Cheng, T. *et al.* CHIR99021 combined with retinoic acid promotes the differentiation of primordial germ cells from human embryonic stem cells. *Oncotarget* **8**, 7814–7826 (2017).
54. Yabe, S. *et al.* Comparison of syncytiotrophoblast generated from human embryonic stem cells and from term placentas. *Proc. Natl. Acad. Sci. USA* **113**, E2598–E2607 (2016).
55. Ye, L. *et al.* Effective cardiac myocyte differentiation of human induced pluripotent stem cells requires VEGF. *PLoS ONE* **8**, (2013).
56. Johnson, W. E., Li, C. & Rabinovic, A. Adjusting batch effects in microarray expression data using empirical Bayes methods. *Biostatistics* **8**, 118–127 (2007).
57. Zhang, Y., Parmigiani, G. & Johnson, W. E. ComBat-seq: Batch effect adjustment for RNA-seq count data. *NAR Genomics Bioinforma.* **2**, lqaa078 (2020).
58. Robinson, M. D., McCarthy, D. J. & Smyth, G. K. edgeR: a Bioconductor package for differential expression analysis of digital gene expression data. *Bioinformatics* **26**, 139–140 (2010).
59. McCarthy, D. J., Chen, Y. & Smyth, G. K. Differential expression analysis of multifactor RNA-Seq experiments with respect to biological variation. *Nucleic Acids Res.* **40**, 4288–4297 (2012).
60. Chen, Y., Lun, A. T. L. & Smyth, G. K. From reads to genes to pathways: differential expression analysis of RNA-Seq experiments using Rsubread and the edgeR quasi-likelihood pipeline. *F1000Research* **5** (2016).
61. Chen, Y., Chen, L., Lun, A. T. L., Baldoni, P. L. & Smyth, G. K. EdgeR 40: powerful differential analysis of sequencing data with expanded functionality and improved support for small counts and larger datasets. *BioRxiv.* https://doi.org/10.1101/2024.01.21.576131 (2024).

Acknowledgements

This work was supported by NIH DK 114453, NIH GM 136309, NSF Graduate Research Fellowship (K.A.L.), and 3M Graduate Fellowship (K.A.L.). Flow cytometry experiments were performed at the University of Minnesota Masonic Cancer Center University Flow Cytometry Resource, which is supported by NIH P30 CA77598. Sequencing was performed at the University of Minnesota Genomics Center Facility (Minneapolis, MN). The authors would also like to thank Dr. Sarah Wernimont for informative discussions and for sharing reagents and BeWo cells.

Author contributions

K.A.L., C.A.S., and S.M.A. conceived and designed the study. K.A.L. performed experiments, data collection, and data analysis. K.A.L., C.A.S., and S.M.A. wrote the manuscript. C.A.S. and S.M.A. supervised and acquired funding for the work.

Competing interests

K.A.L., C.A.S., and S.M.A. have a patent pending for the methods described herein to establish the trophoblast model.

Additional information

Supplementary Information The online version contains supplementary material available at https://doi.org/10.1038/s41598-024-68952-0.

Correspondence and requests for materials should be addressed to S.M.A.

Reprints and permissions information is available at www.nature.com/reprints.

Publisher's note Springer Nature remains neutral with regard to jurisdictional claims in published maps and institutional affiliations.